JOURNAL OF PROPULSION AND POWER
Vol. 25, No. 1, January–February 2009

Large Eddy Simulation of Flow Development in Chamber with Surface Mass Injection

Changjin Lee* and Yang Na†
Konkuk University, Seoul 143-701, Republic of Korea

DOI: 10.2514/1.34980

Motivated by the recent experimental observation of noticeable features of dimplelike surface roughness patterns on the hybrid fuel grain, the authors investigated a cold flow in a porous chamber with surface mass injection through a large eddy simulation technique. The main purpose is to understand the role of turbulent structures in generating those irregular, isolated roughness patterns found on the fuel surface. It was noted that the structural feature of near-wall coherent vortices has been considerably altered by the application of wall injection, resulting in isolated cell-like contours of streamwise velocity distributed all over the horizontal planes close to the wall. This sudden change of contour shape is reminiscent of the roughness patterns observed in the accompanying experiment. The rapid evolution of the kinematical configuration of near-wall turbulence structures is believed to be caused by the effect of vertical momentum given at the wall as in the regression process.

Nomenclature

C_S	=	model coefficient for velocity field
C_T	=	model coefficient for passive scalar
h	=	half-channel height
L_x	=	domain size in streamwise direction
L_y	=	domain size in wall-normal direction, $2h$
L_z	=	domain size in spanwise direction
Pr	=	molecular Prandtl number
p	=	pressure
q_j	=	residual scalar flux vector
R_{uu}	=	two point or autocorrelation of streamwise velocity
Re_h	=	Reynolds number based on inlet bulk velocity and half-channel height
S_{ij}	=	strain rate tensor, $(u_{i,j} + u_{j,i})/2$
T	=	temperature (passive scalar)
T_w	=	wall temperature
t	=	time
U_b	=	inlet bulk velocity
u	=	velocity component in x direction
v	=	velocity component in y direction
w	=	velocity component in z direction
x	=	Cartesian coordinate in streamwise direction
y	=	Cartesian coordinate in wall-normal direction
z	=	Cartesian coordinate in spanwise direction
α_t	=	turbulent diffusivity
Δ	=	filter width
δ_{ij}	=	Kronecker delta function
ν_t	=	turbulent viscosity
τ_{ij}	=	residual stress tensor

Subscripts

b	=	bulk mean quantity
mean	=	averaged quantity over time and spanwise direction

Superscripts

$\langle\,\rangle$	=	grid filter
$\langle\,\rangle_t$	=	test filter
$'$	=	fluctuating component due to turbulence

I. Introduction

HYBRID rockets are attracting much attention these days due to their well-known safety and low development cost. However, to be effectively applied in a wide range of propulsion systems, their low density specific impulse needs to be further improved. Thus, much effort is being made toward devising better ways of enhancing the regression rate of the hybrid fuels in various aspects (Chiaverini et al. [1,2], Wernimont and Heister [3]). Vortex-type rockets [4] can be regarded as one of those successful examples where the residence time is significantly increased by the direct manipulation of the fluid dynamical aspect of the oxidizer flow with help from the early stage numerical analysis [5].

A recent experimental result with polymethyl methacrylate (PMMA) [6] indicated that the combustion process with the enhanced regression rate constantly left isolated, dimplelike surface roughness patterns all over the fuel surface. The appearance of these peculiar cell patterns may be thought of as a consequence of an incomplete combustion process but, interestingly enough, the same behavior persists even in the case of an excessive supply of oxidizer well over the stoichiometric O/F ratio [6]. This fact suggests that the formation of surface roughness patterns detected in a hybrid rocket motor is a realization of the inherent flow instability, which is not usually observed in other types of chemical rockets such as liquid or solid rocket systems. Thus, it is very likely that the formation of cell structures is, to some extent, originated from the modification of boundary layer characteristics of an entering oxidizer flow caused by a blowing effect mainly taking place in the vicinity of the wall during the regression process.

Evans et al. [7] also reported similar cell structures on the fuel surface in their experiment with a N_2O/HTPB (hydroxyl terminated polybutadiene) combination. The average regression rate and the size of the individual cell structure are bigger than those found by Koo and Lee [6]. Even though the magnitude of the mass flow rate of wall blowing coming out of the fuel surface is approximately less than 4% of the oxidizer stream in their study, this amount of blowing seems to be large enough to completely alter the flow characteristics of near-wall turbulence. Although they conjectured that the formation of cell structure is related to the flow transition from laminar to turbulent flows, a detailed description for the physical mechanism has not been proposed.

Presented as Paper 5357 at the 43rd AIAA/ASME/SAE/ASEE Joint Propulsion Conference & Exhibit, Cincinnati, OH, 8–11 July 2007; received 4 October 2007; revision received 27 August 2008; accepted for publication 30 August 2008.

*Professor, Department of Aerospace Engineering, Gwangjin-gu, Hwayang-dong 1. Senior Member AIAA.

†Associate Professor, Department of Mechanical Engineering, Gwangjin-gu, Hwayang-dong 1 (Corresponding Author).

A proper explanation for the formation of those roughness patterns is likely to be important to the understanding of the physics involved in the regression process of the hybrid fuel, but the phenomenon has not been fully understood yet. The main difficulty of investigating the flow inside the hybrid rocket motor is possibly due to the lack of proper instrumentation required for the complex combustion phenomena occurring near the fuel surface. In addition to this measurement restriction, a prohibitively large computational cost required for resolving all the relevant turbulence scales imposed a similar limitation on the numerical simulations. This fact is reflected in the difficulty of predicting the regression process with satisfactory accuracy using currently available turbulence models.

Most of the previous investigations relevant to the solid or hybrid rocket motor dealt with the geometry of a transpired channel assuming that a combustion induced flowfield in rocket motors can be thought of as mass injection from the burning surface. Earlier pioneering experimental works conducted by Yamada et al. [8], Traineau et al. [9], and Dunlap et al. [10] stimulated the research on the injection-driven flow. In their studies, axial mean velocity profiles were measured and compared with the laminar inviscid solution derived analytically by Culick [11]. As noticed by Dunlap et al. [10], the insensitivity of the mean flow to the turbulence could probably be explained by the observation that the flow is mainly governed by the balance between the inertia force and pressure gradient, and therefore, the turbulent shear stress term is not playing a significant role in the mean flow dynamics. Later, Tsai and Liou [12] studied the flow induced by a nonuniform injection experimentally and Balakrishnan et al. [13] explored the effects of compressibility and reviewed the issue of the mean flow transition. Comprehensive literature relevant to the injection-driven flow can be found in [14–16].

Several numerical simulations also have been performed to study the flowfield within a rocket combustion chamber. Most of the earlier numerical studies employed the Reynolds stress or k–ε turbulence models to solve the turbulent flow. Beddini [17] employed a full Reynolds stress turbulence model to analyze the flows in porous channels. Sabnis et al. [18] applied a low Reynolds number k–ε model to predict the flowfield measured by Dunlap et al. [10]. However, Liou and Lien [19] later noted that most of the previous numerical studies with existing turbulence models greatly overpredict turbulence levels. In an effort of obtaining more realistic results, several researchers have extended the previous methodology to the three-dimensional cases [20–23]. However, due to its complex physical nature of the problem, they still had to deal with the Reynolds-averaged Navier–Stokes equation (RANS)-type computations instead of seeking the direct solution of the unsteady Navier–Stokes equations. Even though they successfully demonstrated that computational fluid dynamics can be a very useful research tool in this area and provided very valuable flowfield information such as mean statistics and species concentration, the success was limited because of the limited performance of the turbulence models considered and its inherent assumption of "steady flow." Note that a typical RANS-type computation relies on the Reynolds-averaging concept, and thus has a limitation on effectively presenting the unsteady turbulent fluctuations which have a wide range of length and time scales. Consequently, it is thought to be practically almost impossible to get the physical insight for the formation process of the surface cell structures observed in the experiments directly from those RANS-type studies. Several researchers put much effort into understanding the physics of side injected flows in a more fundamental way. Especially, French research groups concentrated on the flow instability in a solid propellant motor extensively [24–28]. Even though most of their works are more relevant to the idealized solid rocket motor, their detailed analysis on the hydrodynamic instability mechanism is worth noting in the context of flow control in the rocket motor.

With the rapid advance in computer resources, more elaborate attempts to attack injection-driven flows via more reliable numerical methodologies are being made. Nicoud et al. [29] performed a direct numerical simulation to study the effect of a high blowing rate on the wall layer. A substantial reduction in wall shear stress was observed compared to the simple channel flow without wall blowing. Later, extensive numerical investigations based on a large eddy simulation (LES) on nonreacting flows had been performed at the Pennsylvania State University by Apte and Yang [14–16]. Emphasis was put on the transition and the hydrodynamic stability of the flow in the geometry considered by Traineau et al. [9]. Their studies, perhaps, can be considered one of the most realistic numerical works up to date in this configuration and they documented very useful information on turbulence development and acoustic excitation processes in a solid rocket motor with the one end being closed. In the absence of the convection effect of a high speed stream of oxidizer in their study, however, its flow dynamics is not likely to be the same as in the present situation of our study, where the main oxidizer flow is introduced into the chamber and then subsequently interacts with the surface injection.

In the current study, an attempt of LES was made for the turbulent oxidizer flow convecting in a transpired chamber with surface mass injection in order to understand the role of turbulent structures with an objective of explaining the experimentally observed isolated cell patterns, to a reasonable extent, from the fluid mechanics point of view. Thus, a variation of thermodynamic properties accompanied in an actual combustion process was not taken into account here. An LES technique was adapted to compromise between the accuracy and the computational cost with confidence that the detailed, unsteady flowfield information obtained from this simulation can provide the necessary physical insight even in the simplified geometry considered in the present work, because the large-scale turbulent structures which basically govern the major transport phenomena are captured rather accurately. This could be a main advantage of LES over the historically popular RANS-type simulations.

To make the analysis more realistic, the Reynolds number was matched to that of the experiment [6], which, in fact, severely puts a restriction on the grid resolution requirement. Thus, up to 101 million grid points were used for the current numerical simulation to resolve the essential turbulent scales involved. To create a better focus on the near-wall turbulent flow with an acceptable computational cost, a hybrid rocket motor was idealized by a simple channel without considering a chemical reaction. Also, the temperature was treated as a passive scalar with Prandtl number being 1.

In the next section, experimentally observed cell structures will be described in detail followed by a numerical methodology as well as various instantaneous and statistical results.

II. Description of Experimental Observation

As previously mentioned, a recent combustion test with PMMA fuel conducted by Koo and Lee [6] reported a very interesting physical phenomenon produced at the fuel surface. When the combustion was completed, it was found that isolated roughness spots are randomly distributed all over the PMMA surface. Figure 1 shows the typical shape of those cell structures along with the magnified views captured at the end of the rocket motor. The visualization shown in Fig. 1 was made with the use of an opaque acryl plate and an intensity reduction filter (ND8) to control the total amount of light intensity transmitted to a digital camera. The experiment was conducted in pipe geometry with an initial diameter

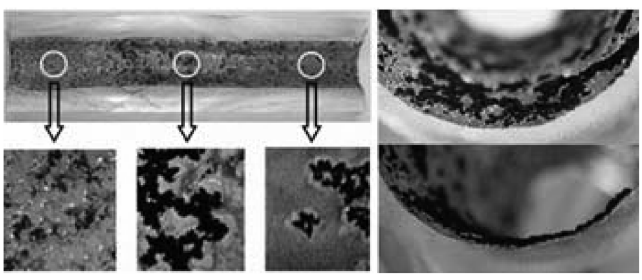

Fig. 1 Surface roughness patterns and their magnified views near the end of a PMMA fuel port.

of the fuel port being 20 mm and the final diameter being 35–40 mm. The fuel port was 300 mm long. The test was conducted for 10 s with an oxidizer (gaseous oxygen) mass flow rate of 0.02 kg/s, which results in the mean inlet velocity of the oxidizer in the range 35–40 m/s. By using the data of the average regression rate, the blowing velocity was calculated to be about 3% of the entering oxidizer velocity. The chamber pressure was maintained at the level of about 300–400 psi. Some of the cell structures were found to be covered with dark, unburned soot, which may be a result from an incomplete combustion, and the typical size of those roughness spots generally increases as the oxidizer convects downstream.

The combustion condition was checked by the use of stoichiometric chemistry to see if the combustion occurred in a fuel-rich condition. The simple calculation of the stoichiometric reaction of PMMA with oxygen gives the stoichiometric O/F ratio of 1.92. Because the actual O/F ratio imposed in the actual test was 4.31, it can be said that the experiment was performed under an oxidizer-rich condition. The fact that dark spots resulting from an incomplete combustion were observed all over the fuel surface even with this high O/F ratio is worth noting.

Figure 2 is a sequence of pictures taken with an equal interval of 1 s. It clearly displays a dramatic change of flow characteristics found on the PMMA surface. The numbers enclosed in the figure indicate the measuring time at which the picture is taken starting from the beginning of the experiment. The first picture (taken at $t = 2$ s) displays a typical streaky pattern of coherent vortices elongated in the main flow direction of the oxidizer. No discernible cell structure patterns are found at this time. However, these patterns (elongated in the streamwise direction) become somehow perturbed at the time of 4 s and very tiny dark spots begin to form in the rear half of the fuel port. It should be noted, however, that the heavy concentration of dark spots in the middle of the fuel is attributed to a sudden expansion of the oxidizer flow from the pressure of 400 to 300 psi in the fuel port. Sometimes dark spots grow into bigger ones and sometimes they are just washed away by the action of strong convection of the oxidizer. Considering the fact that each stage of combustion is characterized by a different regression rate, the observed sudden change of visualized features from a streaky to an isolated cell pattern is more likely to be linked to the structural change of near-wall turbulent structures caused by the increasingly larger regression rate (or equivalently, higher surface injection effect) produced in the later stage of the combustion process.

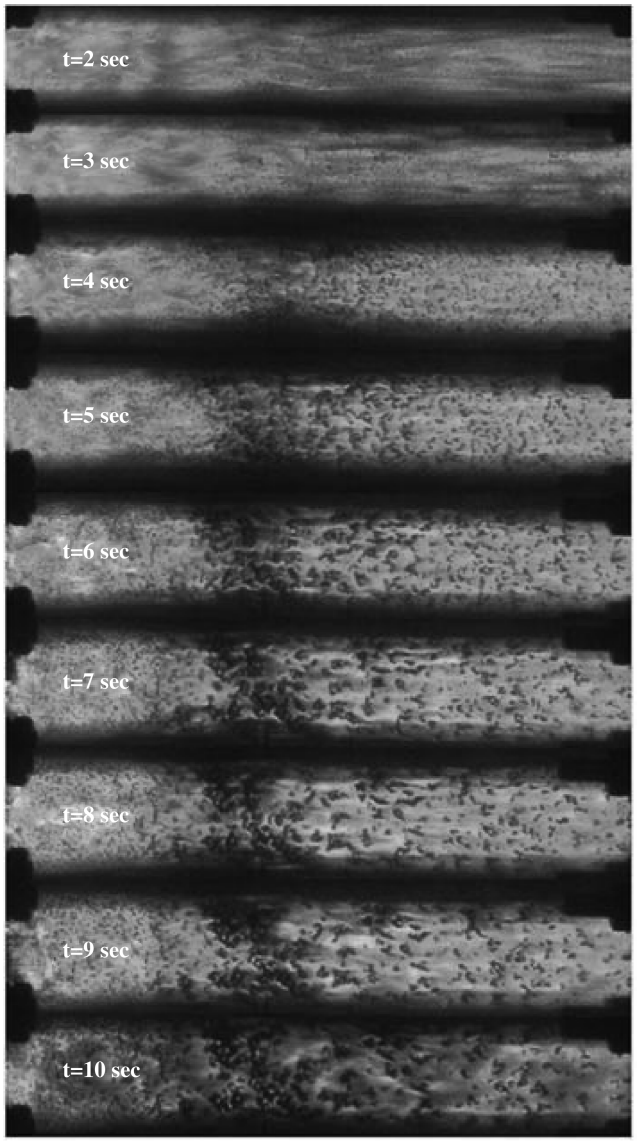

Fig. 2 Sequential changes of near-surface flow patterns during PMMA combustion of [1].

Evans et al. [7] also reported similar transition patterns from smooth to rough surfaces in the experiment with the HTPB/N_2O combination with/without aluminum particles. The mass flow rate of oxidizer N_2O ranges from 0.022 to 0.028 kg/s and the regression rate varies approximately from 0.8 to 1.24 mm/s. The chamber pressure was in the range of 200–300 psi during the stable combustion period. The typical size of the surface cell pattern seems to be generally bigger than that observed in the test of Koo and Lee [6] with PMMA. A possible reason for getting bigger patterns is perhaps the higher flow rate of the oxidizer or the higher regression rate achieved in the experiment of Evans et al. [7]. The previous stability analysis of the French group [24–28] suggests the ratio of the height above the burning fuel and the length of the injecting surface can be viewed as a major parameter that affects the turbulent structure in the injection-driven flow frequently found in a solid rocket motor. In this situation, however, the flow experiences a very complicated process of transition from laminar to turbulent regimes and is likely to be very sensitive to the geometry change during the combustion process. On the other hand, in the hybrid rocket motor, the externally supplied oxidizer enters the fuel port in a fully turbulent state. Thus, the aspect of stability is expected to be somewhat different from that in a solid motor and more careful studies need to be carried out in order to correlate the size of the isolated dimplelike patterns with various flow and geometric parameters.

III. Numerical Methodology

One of the most popular LES models is, perhaps, the dynamic Smagorinsky model (DSM). This model has been successfully applied to a various class of flows for the past 15 years. Even with this proven validity, its excessive dissipative nature prompted a series of further modifications to the model. One such successful effort is the so-called dynamic mixed model (DMM) developed by Zang et al. [30]. This model, which also has been tested for a variety of flows, is known for its generally better performance and robustness than its predecessor, DSM. In addition to the better accuracy, DMM is relatively easy to be incorporated in a physical space with a box filter. A brief summary of the numerical methodology with DMM will be described in the following section but more details can be found in [31].

A. Governing Equation for LES

Considering the fact that the velocity of the oxidizer inside the hybrid motor remained relatively low compared to the sonic velocity in the accompanying experiment [6] (the maximum flow rate of the oxygen is 0.002 kg/s and the corresponding maximum entering velocity is about 40 m/s), it is believed that the cell roughness patterns should be realizable with the assumption of incompressible flow. Thus, the following filtered transport equations for the passive scalar in addition to continuity and momentum equations were considered:

$$\frac{\partial \langle u_i \rangle}{\partial x_i} = 0 \tag{1}$$

$$\frac{\partial \langle u_i \rangle}{\partial t} + \frac{\partial}{\partial x_j}(\langle u_i \rangle \langle u_j \rangle) = -\frac{\partial \langle p \rangle}{\partial x_i} + \frac{\partial}{\partial x_j}(2\nu \langle S_{ij} \rangle - \tau_{ij}) \tag{2}$$

$$\frac{\partial \langle T \rangle}{\partial t} + \frac{\partial}{\partial x_j}(\langle u_j \rangle \langle T \rangle) = \frac{\partial}{\partial x_j}\left(\alpha \frac{\partial \langle T \rangle}{\partial x_j} - q_j\right) \tag{3}$$

Here, the angle bracket denotes the grid filtering operation. To close the governing equations mathematically, LES models for the following residual stress tensor τ_{ij} and the residual heat flux vector q_j should be provided:

$$\tau_{ij} = \langle u_i u_j \rangle - \langle u_i \rangle \langle u_j \rangle, \qquad q_j = \langle T u_j \rangle - \langle T \rangle \langle u_j \rangle \tag{4}$$

Because the DMM of [30] was adopted in the present study, the following procedure was incorporated for the calculation of the turbulent velocity field with a box filtering operation in the physical space:

$$\tau_{ij} - \frac{\delta_{ij}}{3}\tau_{kk} = -2\nu_t \langle S_{ij} \rangle + \left(L_{ij}^m - \frac{\delta_{ij}}{3} L_{kk}^m\right) \tag{5}$$

$$\nu_t = C_s \langle \Delta \rangle^2 \langle S \rangle, \qquad L_{ij}^m = \langle \langle u_i \rangle \langle u_j \rangle \rangle - \langle \langle u_i \rangle \rangle \langle \langle u_j \rangle \rangle \tag{6}$$

In the above equations, the modified Leonard term is explicitly calculated using the filtered flowfield, and the turbulent viscosity ν_t is determined dynamically through the following steps using the test filtering operation denoted by the tilde:

$$C_S = \frac{1}{2\langle \Delta \rangle^2} \frac{M_{ij}(L_{ij} - H_{ij})}{M_{kl} M_{kl}} \tag{7}$$

$$\begin{aligned} M_{ij} &= [\langle \langle S \rangle \langle S_{ij} \rangle \rangle_t - (\langle \langle \Delta \rangle_t / \langle \Delta \rangle) \langle \langle S \rangle \rangle_t \langle \langle S_{ij} \rangle \rangle_t] \\ L_{ij} &= \langle \langle u_i \rangle \langle u_j \rangle \rangle_t - \langle \langle u_i \rangle \rangle_t \langle \langle u_j \rangle \rangle_t \\ H_{ij} &= \langle \langle \langle u_i \rangle \rangle \langle \langle u_j \rangle \rangle \rangle_t - \langle \langle \langle u_i \rangle \rangle \rangle_t \langle \langle \langle u_j \rangle \rangle \rangle_t \end{aligned} \tag{8}$$

The procedure of DMM for getting the velocity field can be extended to the passive scalar in a similar manner for evaluating the residual heat flux vector q_j. As was done for the residual stress tensor, the heat flux vector consists of two terms and the turbulent diffusivity is obtained dynamically as explained in the following:

$$q_j = -\alpha_t \frac{\partial \langle T \rangle}{\partial x_j} + F_j^m \tag{9}$$

$$\alpha_t = C_T \langle \Delta \rangle^2 \bar{S} \qquad F_j^m = \langle \langle T \rangle \langle u_j \rangle \rangle - \langle \langle T \rangle \rangle \langle \langle u_j \rangle \rangle \tag{10}$$

$$C_T = \frac{1}{\langle \Delta \rangle^2} \frac{(F_k - G_k) H_k}{H_k H_k} \tag{11}$$

$$\begin{aligned} F_k &= \langle \langle T \rangle \langle u_k \rangle \rangle_t - \langle \langle T \rangle \rangle_t \langle \langle u_k \rangle \rangle_t \\ G_k &= \langle \langle \langle T \rangle \rangle \langle \langle u_k \rangle \rangle \rangle_t - \langle \langle \langle T \rangle \rangle \rangle_t \langle \langle \langle u_k \rangle \rangle \rangle_t \\ H_k &= \left\langle \langle S \rangle \frac{\partial \langle T \rangle}{\partial x_k} \right\rangle_t - \left(\frac{\langle \langle \Delta \rangle \rangle_t}{\langle \Delta \rangle} \right)^2 \langle \langle S \rangle \rangle_t \frac{\partial \langle \langle T \rangle \rangle_t}{\partial x_k} \end{aligned} \tag{12}$$

Governing equations (1–3) are integrated in time using a semi-implicit procedure [32,33]. The convective term is treated by the third order Runge–Kutta method and the viscous term is integrated by the second order Crank–Nicolson scheme. All the spatial derivatives were conducted by using the second order central difference scheme except for the convective term of Eq. (3). Noting the fact that the central difference scheme applied to the convective term of the passive scalar equation suffers from the numerical instability, a popular quadratic upstream interpolation for convection kinematics (QUICK) scheme [34] was used to effectively suppress the numerical oscillation. The only adjustable parameter in the DMM is the ratio of test to grid filter width, $\tilde{\Delta}/\bar{\Delta}$. From our earlier work, it is shown that the value of 2 for this ratio produced good results [31]. Thus, this value was adopted in the present study. The general accuracy of the present numerical methodology was assessed rigorously in the case of turbulent channel flow by Na [31,33].

B. Computational Geometry and Boundary Condition

The numerical domain is illustrated in Fig. 3. The model rocket motor was idealized by a simple channel and the regression process is approximated by an artificial injection of the fluid at the wall. Because the main scope of the present work is to examine the interaction of the main oxidizer flow with the injected flow prescribed at the wall, which basically occurs in the vicinity of the wall in hybrid rocket motors, the difference in pipe and flat-walled geometry is not believed to deteriorate the validity of the present numerical result in a significant way because the near-wall statistics are known to be very similar in both geometries [35].

To supply physically realistic turbulence to the transpired channel, which is very crucial to the present hybrid motor-type simulation, the flow is continuously recycled inside another channel which is placed just in front of the domain of the main interest adopting the methodology of [36]. This configuration allows the spatial room for developing realistic turbulence economically. The validity of the procedure of generating turbulence using this configuration was also established in [31,33].

A no-slip boundary condition was assumed along the wall except in the second half of the channel where injection is applied. The magnitude of the injected vertical velocity was prescribed to vary linearly from 1% (at $x/h = 13.2$) to 3% (at $x/h = 26$) of the bulk velocity of the oxidizer given at the inlet of the numerical domain by adopting the typical values observed in the experiment [6].

For the calculation of the passive scalar, constant temperatures were maintained along the walls with the lower wall at T_w and the upper wall at $-T_w$. Because the temperature was assumed to be a passive scalar, specifying a higher temperature at a lower wall does not cause any density-driven secondary motions.

A periodic boundary condition was imposed in the spanwise direction and the size of the computational domain was checked by the two-point correlation in this direction. For the domain outlet, the convective boundary condition was specified at the exit to allow turbulence structures to leave the domain with minimal distortion.

C. Numerical Grid

The geometry of the present injection-driven flow contains several regions of non-negligible gradients in the wall-normal direction, which requires careful resolution. Inspecting the gradients of both streamwise velocity and temperature in the vertical direction at

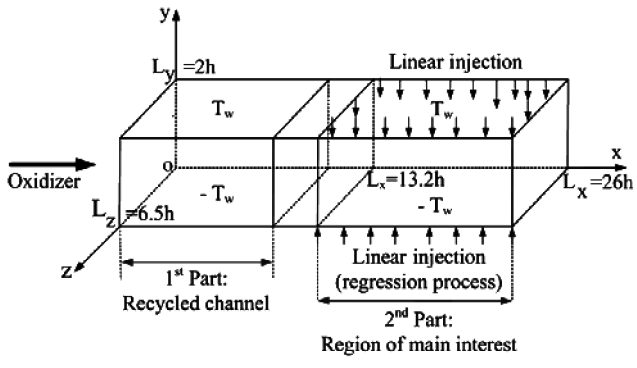

Fig. 3 Schematic of computational domain.

several streamwise locations from the preliminary computations, it was found that a grid stretching using a cosine function was desirable in the wall-normal direction. However, uniform grid spacings were employed in both streamwise and spanwise directions to take advantage of the use of transform methods in the solution of the Poisson equation for pressure.

The Reynolds number based on inlet bulk velocity of the oxidizer and the half-channel height was set to 22,500, which is very close to that of the accompanying experiment [6]. In terms of Reynolds number based on average friction velocity in the recycled channel, this Reynolds number is approximately equivalent to $Re_\tau = 1120$. A relatively high Reynolds number chosen in the present work requires a huge computational expenditure due to the presence of very small-scale turbulence. Thus, a series of computations was conducted with different levels of resolution. Adequacy of the grid resolution was assessed by examining the progressions of mean streamwise velocity and temperature at several representative streamwise locations (Fig. 4). First, these progressions suggest that mean streamwise velocity profiles deviate significantly from that of a nontranspired channel because the mean flow dynamics in the present configuration are significantly different from those in a simple channel. Distributions of mean temperature (Fig. 4b) also showed sizable departure as well. Second, higher resolution consistently improved the prediction of mean variables but the higher resolution in the x direction does not improve the solution if 513 or more grid points are used in this direction. Also, the resolution in the spanwise direction with 513 grid points was checked by examining the two-point correlation data (discussed later in Sec. IV), and it was found that 513 points are generally sufficient to resolve the large-scale turbulent fluctuations in the spanwise direction. Based on the average friction velocity in the recycled channel region, the grid spacing in the streamwise direction was approximately $\Delta x^+ \approx 28.4$ in wall units. In the wall-normal direction, the minimum grid spacing was $\Delta y^+_{\min} \approx 0.075$ at the wall, whereas the maximum grid spacing was $\Delta y^+_{\max} \approx 18.3$ in the middle of the channel. The uniform grid spacing in the spanwise direction was $\Delta z^+ \approx 14.2$ in terms of wall units. In his early LES studies on the turbulent channel, Piomelli [37] showed that wall stress, mean velocity, and Reynolds stress profiles compare well with both experimental and direct numerical simulation even with much coarser grids than the present work for the Reynolds number Re_τ in the range between 200 and 2000. For the sake of saving computational resources, it was decided that any computation with the higher resolution beyond the $1025 \times 193 \times 513$ grid system was not attempted. Because most of the conclusions drawn in the present work are based on instantaneous flowfields rather than quantitative measures of statistical variables, the mesh system with $1025 \times 193 \times 513$ grids (about 101×10^6 grids) is believed to be reasonably good enough for the purpose of the present work.

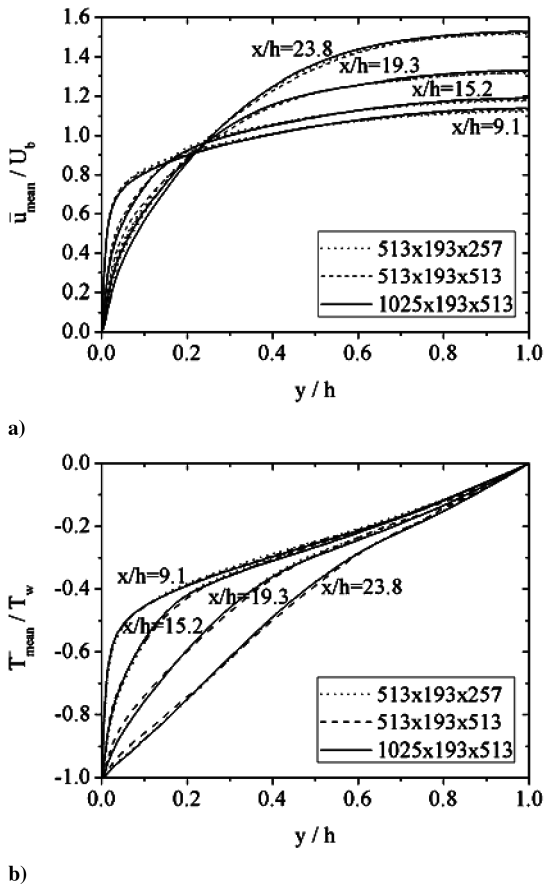

Fig. 4 Comparison of mean statistics of a) streamwise velocity; b) temperature.

For the calculation of statistical quantities, averages were taken over the homogeneous spanwise direction as well as time. Hence, single-point statistics are functions of both x and y. In the present flow configuration, the flow experiences very complex changes due to the strong shear layer developing away from the wall after the injection is applied. This caused slower statistical convergence compared with other simple wall-bounded shear flows. The total averaging time for statistics was $15.4h/U_b$. In line with the purpose of this work, discussions will take place using the instantaneous flowfields and thus, a longer averaging time for the highly smoothed statistics was not pursued for the sake of saving computational resources.

IV. Results

A. Instantaneous Flowfields

Contours of instantaneous streamwise velocity in the (x–z) plane located close to the wall (Fig. 5) clearly show that the structural feature has been significantly altered by the application of wall injection. When the wall blowing is not applied ($x/h < 13.2$), the streamwise velocity contours obviously exhibit high and low speed streaks which are mainly elongated in the main flow direction. The appearance of streaks is well known to be originated from the presence of quasi-streamwise coherent vortices which are convecting downstream in the vicinity of the wall. A sudden change in contour shapes is realized when the wall blowing starts to be applied ($x/h > 13.2$). Instead of the flow patterns that are more elongated in the streamwise direction, the isolated, round-shaped contours become prevalent in this region, which is reminiscent of the surface cell structure patterns found in the experiment [6,7] (Fig. 2). This abrupt change of flow characteristics is believed to be accompanied by the rapid movement of coherent structures away from the wall. Thus, it was decided to investigate the evolution of turbulent structures using a well-established vortex identification method of Zhou et al. [38] (vortice detection is related to eigenvalues of the velocity gradient tensor). A close examination of isocontours of coherent structures displayed in Fig. 6 reveals that the streaky structures generated upstream of wall injection (they tend to be aligned more or less in the main flow direction) are displaced away from the wall, leaving more isolated, round-shaped contours on the fuel surface as their footprints. In addition to this displacement, the shear layer resulting from the intensive mixing of the main flow with the injected fluid contributes to the abundant supply of coherent structures.

Investigation of structural change of near-wall turbulence was further pursued by using isocontours of streamwise velocity near the wall. Figure 7a clearly indicates that wall injection has a significant impact on the evolution of near-wall turbulence. As discussed earlier, streaky patterns are prevalent before the injection but, soon those patterns go through a rapid distortion to become a very agitated or roughened surface. To see the role of wall-normal velocity better, isocontours of streamwise velocity were colored by the magnitude of the wall-normal velocity in Fig. 7b. Again, it is noted that a dramatic change in flow pattern was created by the upward momentum applied at the wall. Even though the wall-normal velocity at the wall is given a constant value in the spanwise direction as an input in the form of boundary condition, a significant corrugation has been found away

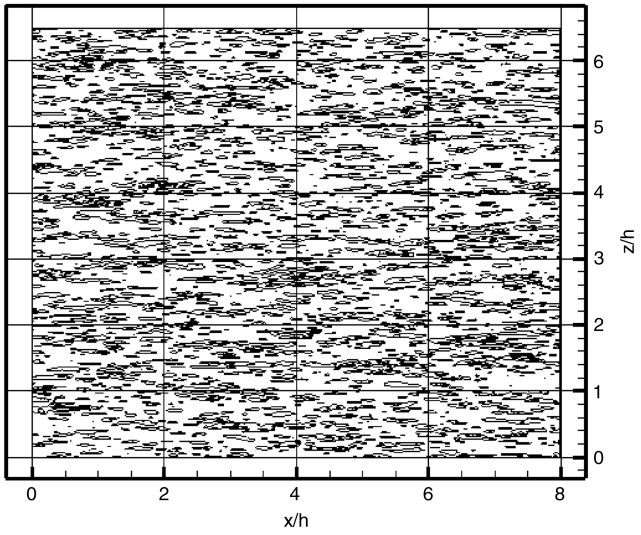

a) Region without wall blowing

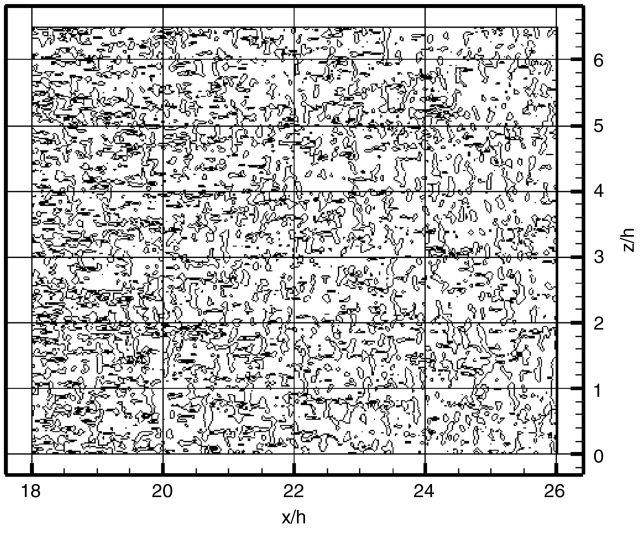

b) Region with wall blowing

Fig. 5 Contours of instantaneous streamwise velocity in the (x–z) plane in the vicinity of the wall ($y/h = 0.0027$).

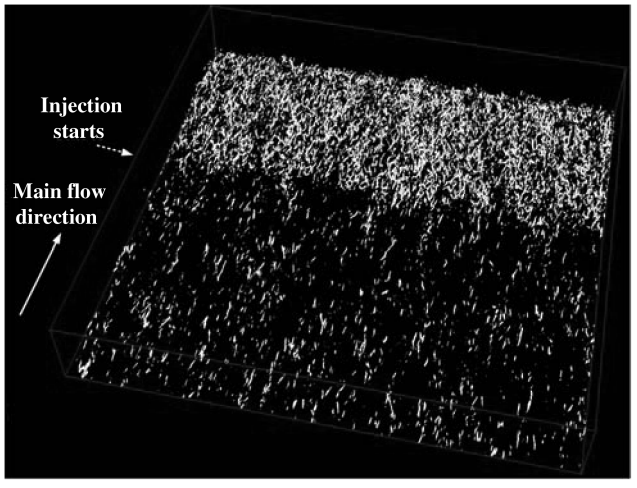

Fig. 6 Isocontours of coherent structures in the region where wall injection begins.

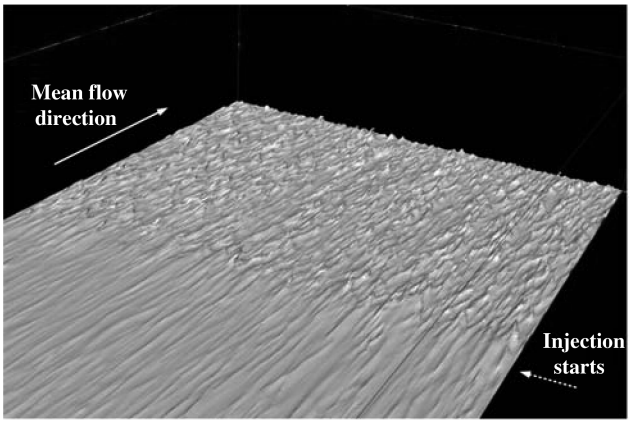

a)

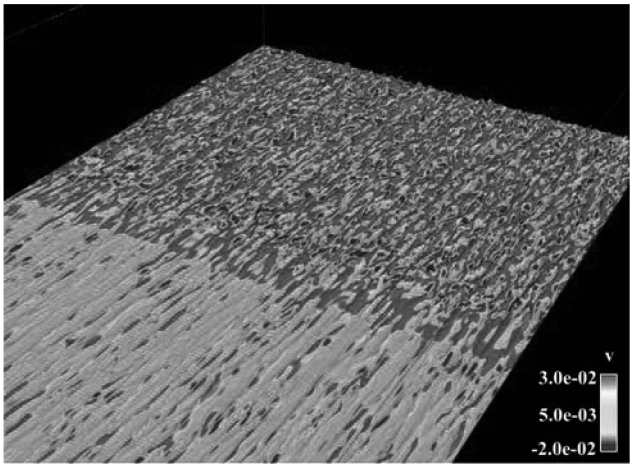

b)

Fig. 7 Isocontours of streamwise velocity in the near-wall region: a) isocontours of streamwise velocity; b) isocontours of streamwise velocity colored by the magnitude of wall-normal velocity.

from the wall. This is obviously caused by the presence of agitated turbulent structures that are convecting downstream. From Fig. 7, it is conjectured that the application of wall blowing immediately modifies the kinematical configuration of turbulence structures such that significant spatial variation in the wall-normal velocity component is rapidly developed away from the wall. This nonuniform distribution may result in an unfavorable environment for maintaining stable diffusion flames in a real situation. At the moment, it is not known whether or not the surface roughness patterns found in the experiment are a direct consequence of the flow instability inherent in the hybrid motor but the present result, at least, provides such a plausible possibility.

Figure 8 shows how differently hydrodynamic and thermal boundary layers react to the wall injection. Because the flow experiences strong acceleration due to the addition of mass through the wall, strong inhomogeneity in the streamwise direction in the region of $x/h > 13.2$ is developed and at the same time, a significant displacement of the hydrodynamic boundary layer is realized. The temperature field shows a generally similar but somewhat distinct behavior in that a relatively farther displacement of the thermal boundary layer away from the wall is evident in Fig. 8b. Because the temperature field was assumed as a passive scalar, this figure suggests that diffusions of momentum and passive scalar take place at different rates.

B. Averaged Flowfields

Mean streamwise velocity and temperature profiles at several streamwise locations (Fig. 9) show that both hydrodynamic and thermal boundary layers are strongly pushed away from the wall

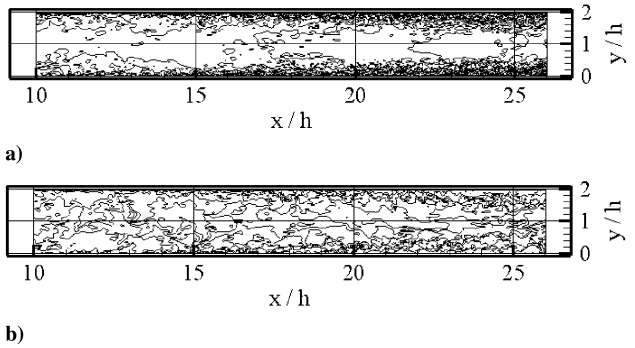

Fig. 8 Contours of instantaneous flowfields in the (x–z) plane in the middle of the computational domain: a) streamwise velocity; b) temperature.

even in the presence of the relatively weak wall injection prescribed in the current work. As is consistent with the behavior shown in Fig. 8, temperature gradient at the wall decreases faster than the velocity gradient. Thus, the friction temperature (not shown here), which is a measure of the ratio of temperature gradient to velocity gradient at the wall, drops significantly in the region with wall injection. This rapid decrease of temperature gradient at the wall will suppress the amount of conduction heat transfer to the surface and eventually deteriorate the subsequent regression rate. Of course, in the actual rocket motor, both convective and radiative heat transfer modes as well as species diffusion and variable density effects will dominate the thermal aspect of the situation and thus, the conduction is not likely to play an important role.

One of the interests in the present study has to do with the behavior of turbulence activities away from the wall. It is expected that a much higher mixing rate is achieved in the middle of the channel in accordance with the significant displacement of boundary layers away from the wall shown in Fig. 9. Figure 10 displays a sequential variation of both turbulent shear stress and heat flux in the wall-normal direction at several locations. Similar to the behavior observed by Apte and Yang in [16], it is again evident that a very strong shear layer resulting from the interaction of the main oxidizer flow with the wall blowing develops away from the wall. In this shear layer, coherent structures multiply very rapidly as shown in Fig. 6 and a high concentration of structures in this region causes a sudden increase in turbulent heat flux as well as in Reynolds shear stress. It is also noted that the location of the maximum heat flux is displaced farther away from the wall than that of the Reynolds shear stress. This behavior is consistent with the findings shown in both instantaneous and statistical results given in Figs. 8 and 9.

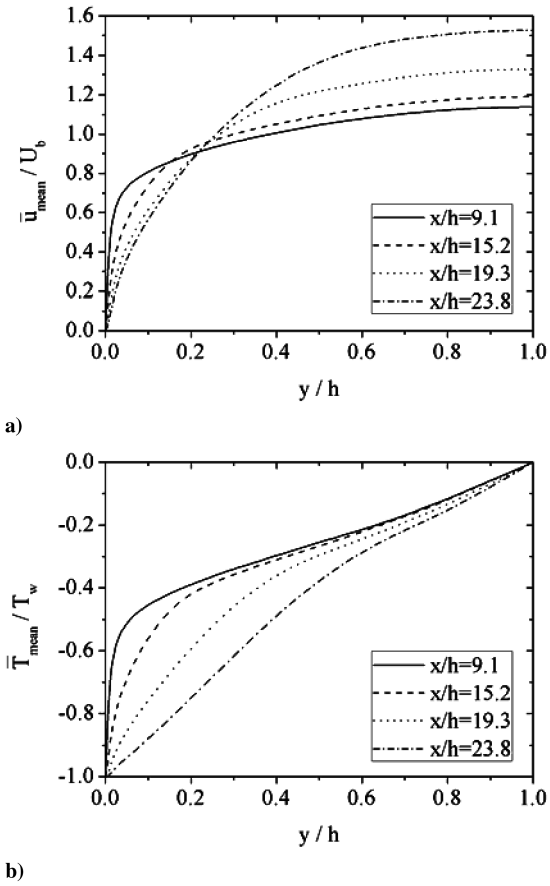

Fig. 9 Mean profiles at several streamwise locations: a) mean streamwise velocity; b) mean temperature.

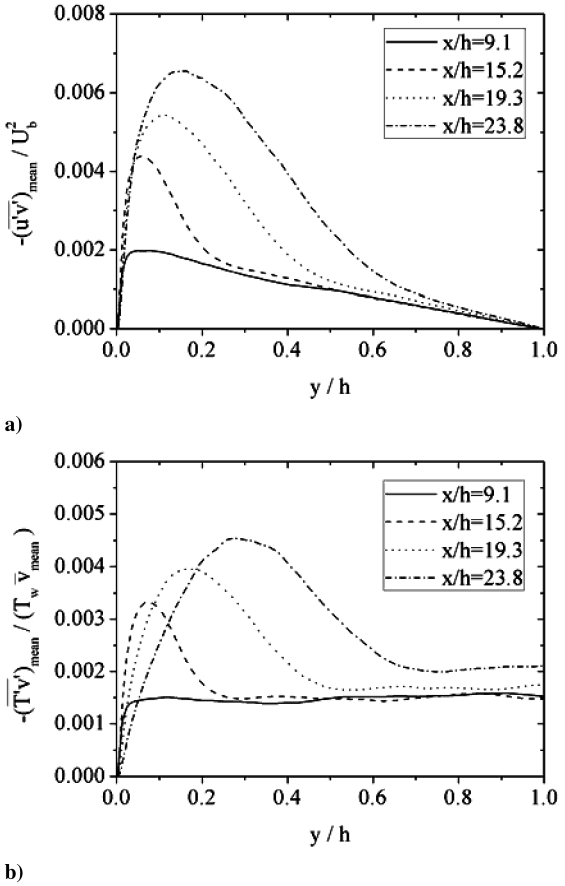

Fig. 10 Profiles of turbulent transport terms at several streamwise locations: a) Reynolds shear stress; b) vertical turbulent heat flux.

Finally, the modification of near-wall turbulent structures in terms of turbulence length scale was examined by inspecting both auto- and two-point correlations of streamwise velocity (Fig. 11). For reference, it should be mentioned that the location of $x/h = 8.1$ corresponds to the station where no injection is applied. In the presence of wall blowing, very large negative excursions develop in the autocorrelation. If Taylor's hypothesis is assumed to be valid here, the behavior shown in the correlation in the time domain can be translated into that in the streamwise direction. Because the averaging time is not long enough, caution must be taken, but the result illustrated in Fig. 11a is somewhat surprising because the typical turbulent boundary layer (i.e., the result at $x/h = 8.1$) is characterized by a monotonic decrease of correlation to a zero value at large separations. It is evident that this unexpected correlation is definitely accompanied by the drastic change in the structural feature of coherent structures. The appearance of large negative values in correlation would probably mean that near-wall turbulent structures are not as elongated as in the upstream if viewed at the given

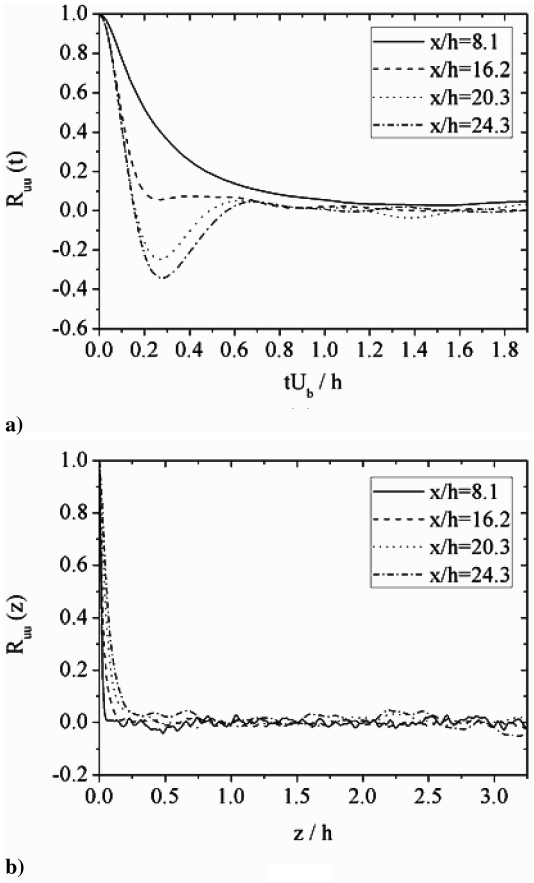

Fig. 11 Correlations of streamwise velocity: a) autocorrelation; b) two-point correlation in the spanwise direction.

wall-normal location. The possible interpretation for this peculiar correlation curve can be made in terms of the change in kinematical configuration of turbulent structures. Because of the wall blowing, downstream heads of turbulent structures tend to be lifted farther away from the wall than their upstream tails similar to the configuration of typical cane or hairpin vortices. Thus, the structures convect downstream with the heads being located higher than their tails. In this tilted, canelike configuration, the coherent vortices can be more closely aligned or packed in the streamwise direction, resulting in a smaller average distance between two consecutive tilted structures than those found in the region without wall blowing. In this hypothetical geometric configuration, the correlation curves can show the excursions around the zero value illustrated in Fig. 11a.

Two-point correlations in the spanwise direction were also examined to assess both the integral length scale and the adequacy of the computational domain size in this direction. Figure 11b shows that all the correlations fall off to zero values at large separations, suggesting that the domain in the spanwise direction is sufficiently large to resolve the largest turbulent eddies. Furthermore, the relatively smoother variation of two-point correlation functions indicates that the spanwise resolution is reasonably good. In the region of wall blowing ($x/h > 13.2$), the average integral scale in the spanwise direction inferred from the correlation curves becomes progressively larger. Thus, it can be conjectured from Fig. 11 that the integral length scale decreases in the streamwise direction, whereas it increases in the spanwise direction by the action of wall injection. These changes in length scales also support the appearance of cell structures found in the experiment.

So far, both instantaneous and mean flowfields were examined to understand the role of wall injection in rapidly modifying the near-wall turbulence. With the evidences presented here, it is strongly believed that the sudden change of kinematical configuration which is manifested by the generation of isolated, round-shaped contours shown in Fig. 5b is strongly related to the cell- type structures observed in the experiments in hybrid motors (Fig. 2).

V. Conclusions

Inspired by the recent experimental observations of irregular, roughened cell patterns found at the hybrid fuel surface, a large eddy simulation was performed in a chamber with surface mass injection with an objective of understanding the origin of those patterns from the viewpoint of fluid mechanics. In particular, emphasis was put on the evolution of near-wall turbulent structures in the presence of wall injection. A dynamic procedure combined with a dynamic mixed model was incorporated and up to 101×10^6 grid points were used to capture the essential features of three-dimensional, unsteady turbulent flowfields at high Reynolds number.

Because of the overwhelming cost of the computation, the present simulation was conducted with several assumptions. A major simplification comes from the assumption of no chemical reaction. Even though this simplification would somewhat limit the validity of the physical interpretation of the current study, the qualitative description of the present work is not likely to be changed much in the real situation because the length scale involved in the combustion process is usually much smaller than that of typical turbulence, resulting in a relatively weak mutual interaction.

Various realizations of instantaneous flowfields clearly show that the structural feature of turbulent vortices was significantly altered by the application of wall injection so that the contours of instantaneous streamwise velocity in the horizontal plane close to the wall produce the patterns similar to those observed in the experiments. Several turbulent statistics and correlations also support the fact that the wall injection drastically changes the characteristics of the near-wall turbulence. Especially, autocorrelation data suggest that the coherent vortices are more closely packed in the streamwise direction in the tilted, canelike configuration with the heads being located higher than their tails. This would result in a smaller average distance between two consecutive tilted structures. Unlike the typical streaky vortices found in the region without wall injection, which are mainly elongated in the streamwise direction, modified coherent structures in this tilted configuration by the action of wall injection are likely to leave isolated, round-shaped footprints of themselves on the fuel surface. Therefore, the sequential change of the patterns observed in the experiment (Fig. 2) is believed to be strongly related to the change in kinematical configuration of near-wall structures caused by the wall blowing.

Considering the limitation of the assumption of cold flow neglecting the effects of both significant density variation and the interaction between the combustion process and turbulence, our next work will consist of more rigorous investigations on these issues.

Acknowledgment

The work of Y. Na was supported by Konkuk University in 2007.

References

[1] Chiaverini, M. J., Serin, N., Johnson, D. K., Lu, Y.-C., Kuo, K. K., and Risha, G. A., "Regression Rate Behavior of Hybrid Rocket Solid Fuels," *Journal of Propulsion and Power*, Vol. 16, No. 1, 2000, pp. 125–132. doi:10.2514/2.5541

[2] Chiaverini, M. J., Kuo, K. K., Peretz, A., and Harting, G. C., "Regression-Rate and Heat-Transfer Correlations for Hybrid Rocket Combustion," *Journal of Propulsion and Power*, Vol. 17, No. 1, 2001, pp. 99–110. doi:10.2514/2.5714

[3] Wernimont, E. J., and Heister, S. D., "Combustion Experiments in Hydrogen Peroxide/Polyethylene Hybrid Rocket with Catalytic Ignition," *Journal of Propulsion and Power*, Vol. 16, No. 2, 2000, pp. 318–326. doi:10.2514/2.5571

[4] Knuth, W. H., Chiaverini, M. J., Sauer, J. A., and Gramer, D. J., "Solid-Fuel Regression Rate Behavior of Vortex Hybrid Rocket Engines," *Journal of Propulsion and Power*, Vol. 18, No. 3, 2002, pp. 600–609. doi:10.2514/2.5974

[5] Knuth, W. H., Gramer, D. J., Chiaverini, M. J., Sauer, J. A., Whitesides, R. H., and Dill, R. A., "Preliminary CFD Analysis of the Vortex Hybrid Rocket Chamber and Nozzle Flow Field," AIAA Paper 98-3351, 1998.
[6] Koo, W., and Lee, C., "The Combustion Characteristics of Oxidizer Flow Change in Hybrid Rocket," *Proceedings of the 2007 Korean Society of Propulsion Engineering Spring Conference*, KSPE, Seoul, 2007, pp. 103–115.
[7] Evans, B., Favorito, N. A., and Kuo, K. K., "Oxidizer-Type and Aluminum Particle Addition Effects on Solid Fuel Burning Behavior," AIAA Paper 2006-4676, 2006.
[8] Yamada, K., Goto, M., and Ishikawa, N., "Simulative Study on the Erosive Burning of solid Rocket Motors," *AIAA Journal*, Vol. 14, No. 9, 1976, pp. 1170–1176. doi:10.2514/3.61451
[9] Traineau, J.-C., Hervat, P., and Kuentzmann, P., "Cold-Flow Simulation of a Two-Dimensional Nozzleless Solid-Rocket Motor," AIAA Paper 86-1447, 1986.
[10] Dunlap, R., Blackner, A. M., Waugh, R. C., Brown, R. S., and Willoughby, P. G., "Internal Flow Field Studies in a Simulated Cylindrical Port Rocket Chamber," *Journal of Propulsion and Power*, Vol. 6, No. 6, 1990, pp. 690–704. doi:10.2514/3.23274
[11] Culick, F. E. C., "Rotational Axisymmetric Mean Flow and Damping of Acoustic Waves in Solid Propellant Rocket Motors," *AIAA Journal*, Vol. 4, No. 8, 1966, pp. 1462–1464. doi:10.2514/3.3709
[12] Tsai, M. K., and Liou, T. M., "Study of Flow Induced by Nonuniform Lateral Injection," *Journal of Propulsion and Power*, Vol. 7, No. 5, 1991, pp. 668–678. doi:10.2514/3.23378
[13] Balakrishnan, G., Linan, A., and Williams, F. A., "Rotational Invscid Flow in Laterally Burning Solid Propellant Rocket Motors," *Journal of Propulsion and Power*, Vol. 8, No. 6, 1992, pp. 1167–1176. doi:10.2514/3.11458
[14] Apte, S., and Yang, V., "Unsteady Flow Evolution in Porous Chamber with Surface Mass Injection, Part 1: Free Oscillation," *AIAA Journal*, Vol. 39, No. 8, 2001, pp. 1577–1586. doi:10.2514/2.1483
[15] Apte, S., and Yang, V., "Unsteady Flow Evolution in Porous Chamber with Surface Mass Injection, Part 2: Acoustic Excitation," *AIAA Journal*, Vol. 40, No. 2, 2002, pp. 244–253. doi:10.2514/2.1666
[16] Apte, S., and Yang, V., "A Large-Eddy Simulation Study of Transition and Flow Instability in a Porous-Walled Chamber with Mass Injection," *Journal of Fluid Mechanics*, Vol. 477, Feb. 2003, pp. 215–225. doi:10.1017/S0022112002002987
[17] Beddini, R. A., "Injection-Induced Flows in Porous-Walled Ducts," *AIAA Journal*, Vol. 24, No. 11, 1986, pp. 1766–1772. doi:10.2514/3.9522
[18] Sabnis, J. S., Gibeling, H. J., and McDonald, H., "Navier-Stokes Analysis of Solid Propellant Rocket Motor Internal Flows," *Journal of Propulsion and Power*, Vol. 5, No. 6, 1989, pp. 657–664. doi:10.2514/3.23203
[19] Liou, T.-M., and Lien, W.-Y., "Numerical Simulation of Injection-Driven Flows in a Two Dimensional Nozzleless Solid Rocket Motor," *Journal of Propulsion and Power*, Vol. 11, No. 4, 1995, pp. 600–606. doi:10.2514/3.23886
[20] Serin, N., and Gogus, Y. A., "Navier-Stokes Investigation on Reacting Flow Field of HTPB/O2 Hybrid Motor and Regression Rate Evaluation," AIAA Paper 2003-4462, 2003.
[21] Cai, G., and Tian, H., "Numerical Simulation of the Operation Process of a Hybrid Rocket Motor," AIAA Paper 2006-4506, 2006.
[22] Yang, Y., Hu, C., Cai, T., and Sun, D., "Instantaneous Regression Rate Computation of Hybrid Rocket Motor Based on Fluid-Solid Coupling Technique," AIAA Paper 2007-5350, 2007.
[23] Farbar, E., Louwers, J., and Kaya, T., "Investigation of Metallized and Nonmetallized Hydroxyl Terminated Polybutadien/Hydrogen Peroxide Hybrid Rockets," *Journal of Propulsion and Power*, Vol. 23, No. 2, 2007, pp. 476–486. doi:10.2514/1.22091
[24] Avalon, G., Casalis, G., and Griffond, J., "Flow Instabilities and Acoustic Resonance of Channels with Wall Injection," AIAA Paper 98-3220, 1998.
[25] Lupoglazoff, N., and Vuillot, F., "Numerical Simulations of Parietal Vortex-Shedding Pheonomenon in a Cold Flow Set-Up," AIAA Paper 98-3220, 1998.
[26] Ugurtas, B., Avalon, G., Lupoglazoff, N., and Vuillot, F., "Numerical Computations of Hydrodynamic Instabilities Inside Channel with Wall Injection," AIAA Paper 99-2505, 1999.
[27] Avalon, G., Ugurtas, B., Grisch, F., and Bresson, A., " Numerical Computations and Visualization Tests of the Flow Inside a Cold Gas Simulation with Characterization of a Parietal Vortex Shedding," AIAA Paper 2000-3387, 2000.
[28] Abu-Irshaid, E. M., Majdalani, J., and Casalis, G., "Hydrodynamic Stability of Rockets with Headwall Injection," *Physics of Fluids*, Vol. 19, No. 2, 2007, p. 024101.
[29] Nicoud, F., Poinsot, T. J., and Minh, H. H., "Direct Numerical Simulation of a Turbulent Flow with Massive Uniform Injection," *10th Symposium on Turbulent Shear Flows*, Pennsylvania State University, University Park, PA, 1995, Vol. 3, pp. 13–18.
[30] Zang, W., Street, R. L., and Koseff, J. R., "A Dynamic Mixed Subgrid-Scale Model and its Application to Turbulent Recirculating Flows," *Physics of Fluids A*, Vol. 5, No. 12, 1993, pp. 3186–3196. doi:10.1063/1.858675
[31] Na, Y., "On the Large Eddy Simulation of Scalar Transport with Prandtl Number up to 10 Using Dynamic Mixed Model," *Journal of Mechanical Science and Technology*, Vol. 19, No. 3, 2005, pp. 913–923.
[32] Na, Y., "Direct Numerical Simulation of Turbulent Boundary Layers with Adverse Pressure Gradient and Separation," Ph.D. Thesis, Department of Mechanical Engineering, Stanford University, Stanford, CA, 1996.
[33] Na, Y., "Direct Numerical Simulation of Turbulent Scalar Field in a Channel with Wall Injection," *Numerical Heat Transfer, Part A, Applications*, Vol. 47, No. 2, 2005, pp. 165–181.
[34] Leonard, B. P., "A Stable and Accurate Convective Modelling Procedure Based on Quadratic Upstream Interpolation," *Computer Methods in Applied Mechanics and Engineering*, Vol. 19, No. 1, 1979, pp. 59–98. doi:10.1016/0045-7825(79)90034-3
[35] Wu, X., and Moin, P., "A Direct Numerical Simulation Study on the Mean Velocity Characteristics in Turbulent Pipe Flow," *Journal of Fluid Mechanics*, Vol. 608, Aug. 2008, pp. 81–112.
[36] Lund, T., Wu, X., and Squires, K. D., "Generation of Turbulent Inflow Data for Spatially-Developing Boundary Layer Simulation," *Journal of Computational Physics*, Vol. 140, No. 2, 1998, pp. 233–258. doi:10.1006/jcph.1998.5882
[37] Piomelli, U., "High Reynolds Number Calculations Using the Dynamic Subgrid-Scale Stress Modesl," *Physics of Fluids A*, Vol. 5, No. 6, 1993, pp. 1484–1490. doi:10.1063/1.858586
[38] Zhou, J., Meinhart, C. D., Balachandra, S., and Adrian, R. J., "Formation of Coherent Packets in Wall Turbulence," *Self-Sustaining Mechanisms of Wall Turbulence*, edited by R. L. Panton, Computational Mechanics Publications, Boston, MA, 1997, pp. 109–134.

J. Oefelein
Associate Editor